INSTITUTE OF PHYSICS PUBLISHING JOURNAL OF PHYSICS D: APPLIED PHYSICS

J. Phys. D: Appl. Phys. **36** (2003) 3079–3088 PII: S0022-3727(03)64774-1

Alloying element vaporization during laser spot welding of stainless steel

X He[1], T DebRoy[1] and P W Fuerschbach[2]

[1] Department of Materials Science and Engineering, The Pennsylvania State University, PA, USA
[2] Joining and Coating Department, Sandia National Laboratories, Albuquerque, NM, USA

Received 14 June 2003
Published 19 November 2003
Online at stacks.iop.org/JPhysD/36/3079

Abstract

Alloying element loss from the weld pool during laser spot welding of stainless steel was investigated experimentally and theoretically. The experimental work involved determination of work-piece weight loss and metal vapour composition for various welding conditions. The transient temperature and velocity fields in the weld pool were numerically simulated. The vaporization rates of the alloying elements were modelled using the computed temperature profiles. The fusion zone geometry could be predicted from the transient heat transfer and fluid flow model for various welding conditions. The laser power and the pulse duration were the most important variables in determining the transient temperature profiles. The velocity of the liquid metal in the weld pool increased with time during heating and convection played an increasingly important role in the heat transfer. The peak temperature and velocity increased significantly with laser power density and pulse duration. At very high power densities, the computed temperatures were higher than the boiling point of 304 stainless steel. As a result, evaporation of alloying elements was caused by both the total pressure and the concentration gradients. The calculations showed that the vaporization occurred mainly from a small region under the laser beam where the temperatures were very high. The computed vapour loss was found to be lower than the measured mass loss because of the ejection of tiny metal droplets owing to the recoil force exerted by the metal vapours. The ejection of metal droplets has been predicted by computations and verified by experiments.

1. Introduction

During laser welding of many important engineering alloys, pronounced vaporization of volatile alloying elements takes place from the weld pool surface when the weld pool temperatures are very high [1–16]. When this temperature is higher than the boiling point, the pressures at the weld pool surface can be greater than the ambient pressure. This excess pressure provides a driving force for the vaporization. The loss of alloying elements can result in significant changes in the microstructure and degradation of mechanical properties of weldments [9–14]. Moon and Metzbower [9] investigated the change of properties of aluminium alloy before and after welding using a CO_2 laser with He gas shield. They found that the tensile properties of the welds were inferior to the base metal, mainly because of magnesium depletion, loss of strain hardened structure, and porosity. Cieslak and Fuerschbach [10] investigated the property change of aluminium alloys 5456 and 5086. They found that the hardness of weld metal was lower than the base metal due to magnesium vaporization. The loss of hardness was attributed to a reduction in the solid solution strengthening effect as a result of a lower magnesium concentration. In the electronics industry, where components are often processed in a clean room environment, discharge of metal vapours is not acceptable. During laser-assisted joining of components, evaporation of alloying elements needs to be minimized. Therefore, a quantitative understanding of the evaporation of alloying elements is important in the welding of engineering alloys.

During welding of stainless steel, the main constituents of the metal vapour are iron, manganese, chromium, and nickel [8, 12–15]. In a high-manganese stainless steel, such

as AISI 201, iron and manganese were the prominent vapour species in the welding environment. In order to have a quantitative understanding of vaporization of weld metal, a comprehensive model is needed. Aden *et al* [17] investigated the laser-induced vaporization from steel and aluminium surfaces as a function of laser intensity and material properties. A material-dependent minimum laser intensity above which no further expansion of the metal vapour occurs was discussed. However, the model did not take into account the flow of liquid metal in the weld pool or the detailed heat transfer in the weldment. A theoretical model was developed by Dilthey *et al* [18] to describe the vaporization of alloying elements during laser welding. Two important processes were analysed, the diffusion of alloying elements from the interior to the weld surface and their subsequent vaporization from the weld pool surface. Both the models ignored the condensation of the metal vapour. Anisimov [19] and Knight [20] derived expressions for the vapour temperature, density, velocity, and extent of condensation by solving the equations of conservation of mass, momentum, and energy in a thin layer adjacent to the liquid–vapour interface, known as the Knudsen layer. Their approach has been incorporated into vaporization models [11, 12] to calculate the laser-induced vaporization rate.

When the weld pool temperatures are very high, the escaping vapour exerts a large recoil force on the weld pool surface, and as a consequence, tiny liquid metal particles may be expelled from the weld pool. Thus, in addition to vaporization of alloying elements, ejection of metal particles may also take place when a high power laser beam is used for welding. The expulsion of liquid metal is not acceptable during welding, since the metal loss can adversely affect the weld geometry and weldment properties. Expulsion of liquid metal has also been reported in [21–24]. Chun and Rose [21] irradiated an aluminium target with a Nd-doped glass laser and found that as much as 90% of the material lost was removed from the molten pool as liquid. The fraction of material lost as liquid depended on the laser pulse characteristics and material properties. Von Allmen [23] suggested that the vapour pressure acts like a piston on the liquid weld pool and forces liquid metal out of the cavity. Basu and DebRoy [24] examined the conditions for the initiation of liquid-metal expulsion during laser irradiation experimentally and theoretically. They proposed that when the vapour recoil force exceeds the surface tension force of the liquid metal at the periphery of the weld pool, liquid expulsion takes place.

The work presented in this paper was conducted to quantitatively understand the vaporization rate of alloying elements during laser spot welding. The temperature field used to calculate the vaporization rate was obtained from a well-tested comprehensive three-dimensional transient numerical model [11–15, 25–29]. Using the computed temperature fields, vapour composition and total mass loss due to vaporization of various alloying elements resulting from both concentration- and pressure-driven transport were calculated. Both vaporization and condensation were considered in the model. The experimentally determined weld pool dimensions, vapour composition and overall vaporization loss were compared with the corresponding modelling results. The possibility of metal expulsion was also examined experimentally and theoretically.

2. Experimental procedure

Several 304 stainless steel welds were fabricated at the Sandia National Laboratories. The steel had the following composition: 1 wt% Mn, 18.1 wt% Cr, 8.6 wt% Ni, 0.69 wt% Si, 0.046 wt% C, 0.012 wt% P, 0.003 wt% S, and balance Fe. A Raytheon SS 525 pulsed Nd : YAG laser was used for laser spot welding with pulse energies of 2.1 J, 3.2 J, and 5.9 J and pulse durations of 4.0 ms and 3.0 ms, respectively. No temporal pulse shaping was employed. The laser beam was focused inside the quartz tube with a 100 mm focal length lens. For each combination of energy and duration, the laser beam was defocused to different extents to obtain various spot diameters and power densities. Individual spot welds from a pulsed laser beam were made on 3 mm $\times$ 10 mm $\times$ 17 mm EDM wire-cut samples. Up to 15 individual spot welds were made on each of the samples. The laser spot size was measured with 50 μm Kapton film using the method described elsewhere [30]. Longitudinal metallographic cross-section measurements through several collinear welds for each plate were averaged to determine weld pool width and depth. The mass loss was experimentally determined by weighing each specimen before and after welding with a Metler MT5 microbalance. To increase the accuracy of the weight loss measurements, the reported mass loss per pulse is the average of the 15 spot welds made on each sample.

In order to determine the concentration of various alloying elements in the vapour, during laser spot welding, a cylindrical 6 mm inner diameter by 25 mm long open-ended quartz tube was placed co-axial to the laser beam and right above the 304 stainless steel samples. The vaporized elements were collected as condensation on the interior surface of the tube. The quartz tube samples were examined using a JEOL 8600 electron microprobe x-ray analyser to determine the vapour composition. The evaporation products had the consistency of fine dust. The quartz tubes were broken and a suitable fragment from each experiment was mounted to expose the deposit. Due to the geometry of the samples and their highly porous nature, the probe was not operated in an automated mode. Instead, a series of spot measurements of the K-values (count rate ratios of unknown to standards) were made on each sample. The K-value measurements were converted to approximate oxide ratios and averaged together for each sample.

3. Mathematical modelling

3.1. Transient temperature profiles

A well-tested transient heat transfer and fluid flow model was used to calculate the temperature and velocity fields in the weld pool both during heating and cooling. The assumptions, model framework, and the solution procedure have been described in detail in recent papers [25, 26] and are not repeated here. The computed temperature fields as a function of time were then used to calculate the vaporization rates of alloying elements. The data used for calculations [30–34] are presented in table 1.

3.2. Vaporization due to concentration gradient

At the weld pool surface, the concentrations of the alloying elements in the vapour are higher than those in the bulk

shielding gas. The vaporization flux of element i, J_{ci}, can be defined as:

$$J_{ci} = K_{gi}\left(M_i \frac{a_i P_i^0}{RT_l} - C_i^b\right) \quad (1)$$

where K_{gi} is the mass transfer coefficient of element i, M_i is the molecular weight of the element i, a_i is the activity of element i in the liquid metal, P_i^0 is the equilibrium vapour pressure of element i over its pure liquid, R is the gas constant, T_l is the temperature at the weld pool surface, and C_i^b is the concentration of element i in the shielding gas, which is significantly lower than the concentration at the weld pool surface. The mass transfer coefficient between the weld pool surface and the shielding gas is calculated from the graphical results of Schlunder and Gniclinski [35] for a jet impinging on a flat surface and is given by

$$K_{gi} = \frac{2Pr^{0.42}Re^{0.5}D_i}{d}\left(1 + \frac{Re^{0.55}}{200}\right)^{0.5} \times \left[0.483 - 0.108\frac{r}{d} + 7.71 \times 10^{-3}\left(\frac{r}{d}\right)^2\right] \quad (2)$$

where Pr is Prandtl number, Re is the Reynolds number at the nozzle exit, D_i is the average diffusivity of element i in the shielding gas at average temperature T_{av}, d is the diameter of the nozzle, and r is the radial distance on the weld pool surface.

Table 1. Data used for calculations [30–34].

Property/parameter	Value
Density of liquid metal (kg m^{-3})	7.2×10^3
Absorption coefficient	0.27
Effective viscosity (kg m^{-1} s^{-1})	0.1
Solidus temperature (K)	1697
Liquidus temperature (K)	1727
Enthalpy of solid at melting point (J kg^{-1})	1.20×10^6
Enthalpy of liquid at melting point (J kg^{-1})	1.26×10^6
Specific heat of solid (J kg^{-1} K^{-1})	711.8
Specific heat of liquid (J kg^{-1} K^{-1})	837.4
Thermal conductivity of solid (J m^{-1} s^{-1} K^{-1})	19.26
Effective thermal conductivity of liquid (J m^{-1} s^{-1} K^{-1})	209.3
Temperature coefficient of surface tension (N m^{-1} K^{-1})	-0.43×10^{-3}
Coefficient of thermal expansion	1.96×10^{-5}
Surface tension coefficient (N m^{-1})	1.872

3.3. Vaporization due to pressure gradient

During laser welding, the peak temperature reached on the weld pool surface often exceeds the boiling point of the alloy. As a result, the vapour pressure at the weld pool surface can be higher than the ambient pressure, and the excess pressure provides a driving force for the vapour to move away from the surface. Therefore, the convective flux of the vaporized elements, driven by the excess pressure, is an important contributor to the overall vaporization flux.

The velocity distribution functions of the vapour molecules, f_1, f_2, and f_3, escaping from the weld pool surface at various locations are shown schematically in figure 1. On the weld pool surface, the molecules cannot travel in the negative direction, and as a consequence, the velocity distribution is half-Maxwellian. Close to the weld pool, there exists a space of several mean free paths length, known as the Knudsen layer, at the outer edge of which the velocity distribution just reaches the equilibrium distribution. Considering the velocity distribution functions, the rate of vaporization and condensation were calculated based on the works of Anisimov [19] and Knight [20] by solving the equations of conservation of mass, momentum, and kinetic energy. The detailed procedure for the calculation of vaporization flux due to pressure gradient, J_{pi}, is available in the paper by Mundra and DebRoy [12] and is not presented here.

3.4. Overall vaporization rate and weight loss due to vaporization

The total vaporization flux for element i is the sum of the diffusion-driven flux, J_{ci}, and the pressure-driven vapour flux, J_{pi}, and can be given by

$$J_i = J_{ci} + J_{pi} \quad (3)$$

The vaporization rate of element i is obtained by integrating the vapour flux over the entire weld pool surface, and the total vaporization rate of all the elements is given by

$$G = \sum_{i=1}^{n} G_i = \sum_{i=1}^{n} \iint_s J_i \, dx \, dy \quad (4)$$

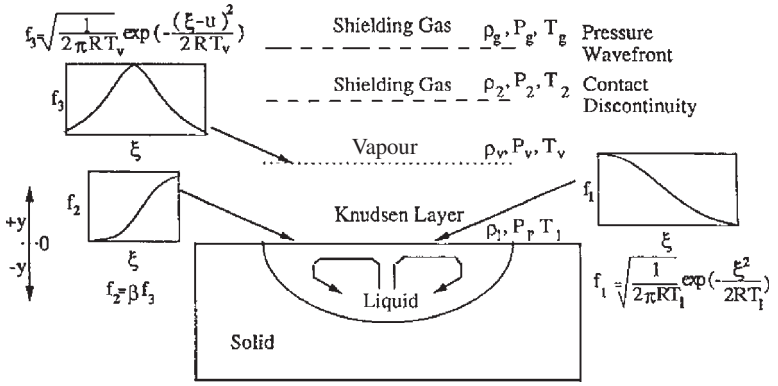

Figure 1. A schematic diagram of the velocity distribution functions in the Knudsen layer and in adjacent regions.

where s indicates the weld pool surface. The total weight loss of element i can be calculated by

$$\Delta W_i = \sum_t \iint_s J_i \Delta t \, \mathrm{d}x \, \mathrm{d}y \tag{5}$$

where Δt is the time step.

4. Results and discussion

4.1. Computed temperature fields and weld pool geometry

Figures 2(*a*)–(*c*) show the computed temperature and velocity fields as a function of time. The liquid metal motion in the weld pool is driven mainly by the surface tension force and to a much lower extent by the buoyancy force. Because of the negative values of the temperature coefficient of surface tension, the surface tension drives the liquid metal from the centre to the periphery at the top surface of the weld pool. As a result, the weld pool becomes wide and shallow. During the initial period of laser spot welding, the weld pool grows rapidly in size and the temperatures increase with time. After the laser is switched off, the temperatures decrease rapidly and consequently the weld pool begins to shrink. The maximum velocity of liquid in the weld pool is 0.73 m s^{-1} after 3 ms. This velocity decreases rapidly after the laser is switched off. The maximum velocity is reduced to 4.5 mm s^{-1} 2.0 ms after the laser is switched off. The computed results show that it takes about 3.55 ms after the power is switched off for the weld pool to solidify completely.

The rate of heat loss per unit area from the pool surface, h_v, owing to vaporization can be expressed as

$$h_v = \sum_{i=1}^{n} J_i \Delta H_i \tag{6}$$

where n is the number of alloying elements, ΔH_i is the enthalpy of vaporization [36] of the element i and J_i is the vaporization flux [37] of element i:

$$J_i = \frac{\lambda P_i}{\sqrt{2\pi M_i RT}} \tag{7}$$

where P_i is the vapour pressure of i over the alloy, M_i is the molecular weight of species i, R is the gas constant, T is the temperature, and λ is a positive constant that accounts for the inevitable condensation of a portion of the vaporized atoms at atmospheric pressure. When the vaporization occurs under perfect vacuum, the value of λ becomes 1. The evaporation flux calculated by the Langmuir equation is usually an order of magnitude higher than the actual rate at 1 atm pressure [5, 8]. Therefore, the value of λ was taken as 0.1 for the calculation of evaporation flux in this paper. Computed peak temperature versus time plots both considering and ignoring the heat of vaporization are presented in figure 3. The heat loss due to vaporization per unit area was much smaller than the heat flux absorbed from the laser beam because of the high power density used in the experiments. As a result, the cooling effect of vaporization was not pronounced; i.e. vaporization did not reduce the surface temperatures significantly. For a typical experimental condition considered in figure 3, i.e. 1967 W, 3 ms duration pulse, and 0.428 mm laser beam radius, the maximum value of peak temperature attained at the end of the pulse was 3205 K when the cooling effect of vaporization was ignored and 3174 K when the effect was considered. For a 530 W laser beam of 0.171 mm radius pulsed for 4 ms, the peak temperatures were 3058 K and 3047 K when the cooling effect was ignored and when the effect was considered, respectively. Thus, under the conditions of the current experiments, the

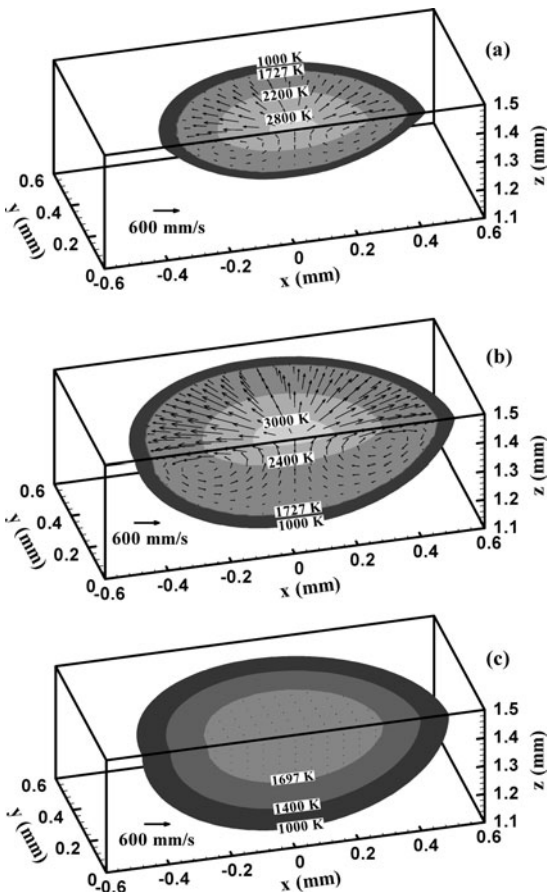

Figure 2. Computed temperature and velocity fields at different times: (*a*) $t = 1$ ms, (*b*) $t = 3$ ms and (*c*) $t = 5$ ms. Laser power: 1967 W, pulse duration: 3.0 ms, and spot radius: 0.428 mm.

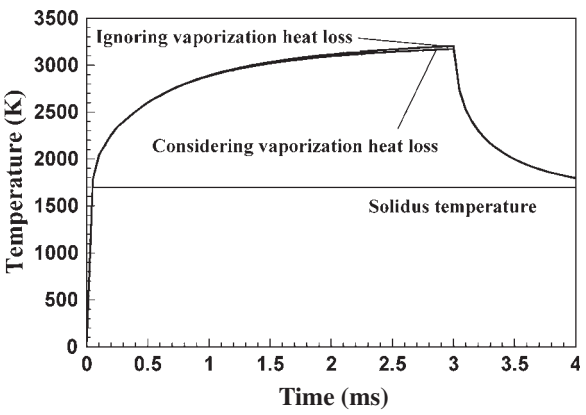

Figure 3. Computed weld thermal cycles on the top surface of the weld pool. The solid horizontal line indicates solidus temperature. Laser power: 1967 W, pulse duration: 3.0 ms, and beam radius: 0.428 mm.

heat loss owing to vaporization was much smaller than the power density of the beam and the vaporization of alloying elements did not significantly affect the computed surface temperatures.

Figure 4 shows changes in the computed temperatures at various monitoring locations, which are indicated as points 1, 2, 3, and 4 in the small figure. These locations represent distances of 0, 0.125, 0.175, and 0.225 mm from the axis of the laser beam, as shown in the figure. There are several special features of interest. First, the temperatures reach very high values near the laser beam axis. It is to be noted that the peak temperature can exceed the boiling point of the alloy, i.e. the equilibrium vapour pressure at the liquid surface can be higher than 1 atm. Second, the computed results also indicate that the heating rates vary significantly, depending on the location. Finally, as the weld metal cools, the spatial variation of the cooling rates within the solid metal is much smaller than the spatial variation in the heating rates. These features of temperature and the temperature distribution at the weld pool surface are of interest in examining the vaporization of alloying elements from the weld pool.

In the weld pool, heat is transported by a combination of convection and conduction mechanisms. The relative importance of convection and conduction in the overall transport of heat can be evaluated from the value of the Peclet number, *Pe*, which is defined by

$$Pe = \frac{u\rho C_p L_R}{k} \tag{8}$$

where u is the velocity, ρ is the density, C_p is the specific heat, L_R is the characteristic length, taken as the pool radius at the top surface of the weld pool, and k is the thermal conductivity. When *Pe* is less than 1, the heat transport within the weld pool occurs primarily by conduction. When *Pe* is much higher than 1, the convective heat transport is the primary mechanism of heat transfer. Figure 5 shows the change of Peclet number with time. It can be seen that at the beginning of the pulse cycle, the Peclet number is low and conduction is the primary mechanism of heat transfer. With time, the Peclet number increases and convection becomes a more important heat transport mechanism in the weld pool. When the pulse is switched off, the Peclet number drops to a very low value very quickly and conduction becomes the main mechanism of heat transfer again.

The variation of peak temperature and maximum velocity with power density is shown in figure 6. Both the peak temperature and the maximum velocity represent the highest values in the weld pool at the end of the pulse. The high maximum velocity at high power densities means a more dominant role of convection at high power densities. The experimentally determined weld pool cross sections are compared with the corresponding computed values under two welding conditions in figure 7. It is observed that the calculated weld pool geometry and dimensions agree well with the experimental results. Experimentally measured and computed values of weld pool depth and width at various other laser

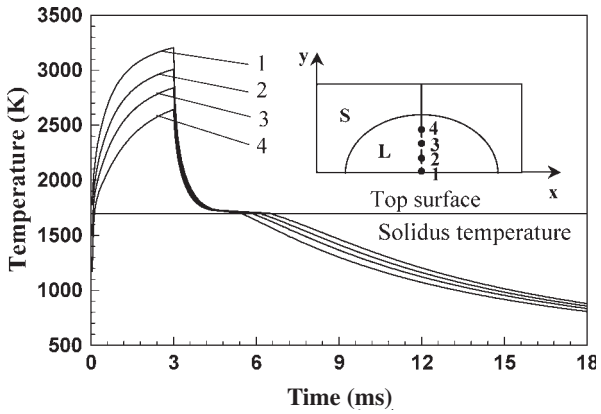

Figure 4. Computed weld thermal cycles at various locations on the top surface of the weld pool. Distance from the weld centre: 1: 0.0 mm, 2: 0.125 mm, 3: 0.175 mm, and 4: 0.225 mm, as shown in the small figure. The solid horizontal lines indicate solidus temperature. Laser power: 1967 W, pulse duration: 3.0 ms, and beam radius: 0.428 mm.

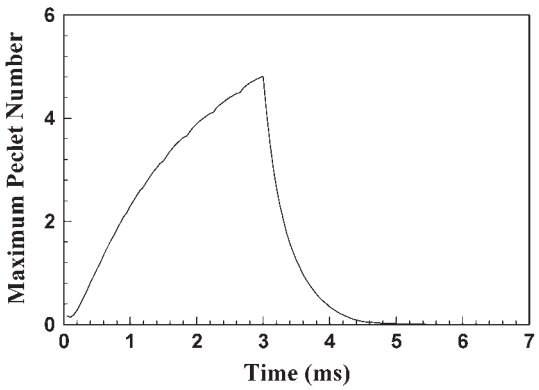

Figure 5. The variation of Peclet number with time. Laser power: 1967 W, pulse duration: 3.0 ms, and beam radius: 0.428 mm.

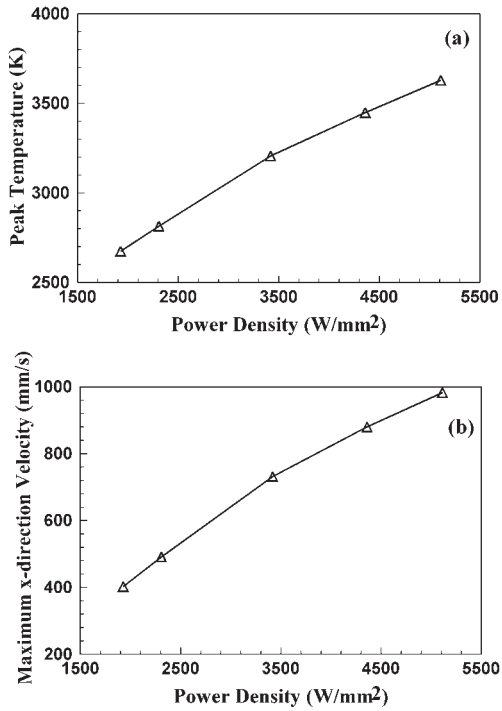

Figure 6. The effects of laser power density on (*a*) the computed peak temperatures and (*b*) the computed maximum velocity. Laser power: 1967 W and pulse duration: 3.0 ms.

power densities are presented in table 2. The total power was kept constant at 530 W while the beam radius was varied to obtain different power densities. It can be seen that the calculated weld pool depth and width show fair agreement with the experimental results.

4.2. Mass loss

Because the weld pool surface temperatures reach high values, pronounced evaporation of alloying elements takes place during high-power laser spot welding. Figure 8 shows the computed temperature distribution and various vapour fluxes at the weld pool surface after 3.0 ms. The total vapour flux is the sum of the fluxes of individual alloying elements resulting from both pressure-driven and concentration difference-driven fluxes. The results show that the distribution patterns of vapour fluxes are similar to the surface temperature profiles. This similarity is anticipated since the vapour fluxes are strongly affected by temperature. The primary driving force for vaporization is the total pressure gradient at temperatures higher than the boiling point. At lower temperatures, the vapour flux is driven mainly by diffusion in the gas phase outside the liquid pool. The calculated results show that most of the vaporization occurs from a small region near the centre of the beam–work-piece interaction zone, where the weld pool surface temperatures are very high as observed from figure 8(*a*). The diameter of this active region is approximately 0.6 mm, as can be observed from figures 8(*b*)–(*h*). This dimension is comparable with but somewhat smaller than the diameter of the laser beam at the focal point.

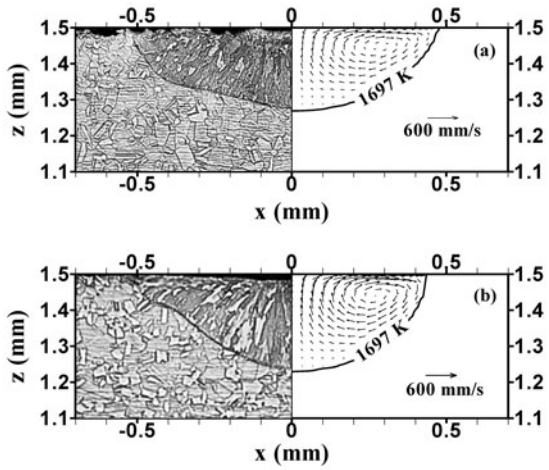

Figure 7. Experimental and calculated weld pool cross sections. (*a*) Laser power: 1967 W, pulse duration: 3 ms, and beam radius: 0.521 mm. (*b*) Laser power: 1507 W, pulse duration: 4 ms, and beam radius: 0.389 mm.

From the computed vapour fluxes presented in figures 8(*e*)–(*h*), it can be seen that iron is the dominant vaporizing species, followed by chromium and manganese. The equilibrium vapour pressure data used for the calculations are presented in the appendix. Although manganese has the highest vapour pressure over its pure liquid, its concentration in 304 stainless steel is much lower than those of iron and chromium. Manganese only accounts for 1.0% of the stainless steel composition, while iron and chromium are present at 72.3% and 18.1%, respectively. The lower concentration results in the lower vapour flux of manganese compared with iron and chromium over 304 stainless steel.

The vapour composition was also determined from the experiments. The concentrations of different elements in the vapour obtained from both experiments and calculations are presented in figure 9. Iron and chromium were the main vaporizing species. It is also observed that the calculated concentrations of various vaporizing species agree well with those obtained from measurements. The experimentally determined and the calculated concentrations of different alloying elements in the vapour are presented in table 3 for various welding conditions. The change in the concentrations of the main vaporizing species, i.e. iron and chromium, with power density is shown in figure 10. Generally, as the power density increases, the concentration of iron in the vapour increases. This is mainly because the slope of the vapour pressure versus temperature plot for iron is steeper than those of the other alloying elements. For a similar reason, the concentration of chromium in the vapour condensate increases slightly with power density.

The calculated mass loss due to evaporation is compared with the experimental results of mass loss at various power densities in figure 11. Some additional results are also presented in table 4 for completeness. As the laser power density increases, the temperature at the weld pool surface exceeds the boiling point of the steel. As a result, the total vaporization loss increases significantly due to pressure-driven vaporization. However, it can be observed that the experimental weight loss is always higher than the computed mass loss due to vaporization. There are two possible reasons for this discrepancy. First, in a complex modelling effort such as the present research, the accuracy of the modelling results must be carefully considered. In other words, a possibility that all the mass loss is attributable to the vaporization of alloying elements and the model consistently underpredicts the vaporization loss cannot be ruled out. Second, it is conceivable that in addition to vaporization, mass loss also occurs due to ejection of metal droplets. Both these possibilities are examined next.

Table 2. Calculated and experimental weld pool dimensions for different welding conditions.

		Depth (mm)		Width (mm)	
Spot radius (mm)		Calculated	Experimental	Calculated	Experimental
530 W,	0.159	0.202	0.190	0.512	0.625
4.0 ms	0.210	0.199	0.267	0.536	0.416
pulse	0.272	0.181	0.117	0.550	0.550
	0.313	0.170	0.092	0.576	0.519
	0.433	0.130	0.058	0.602	0.477

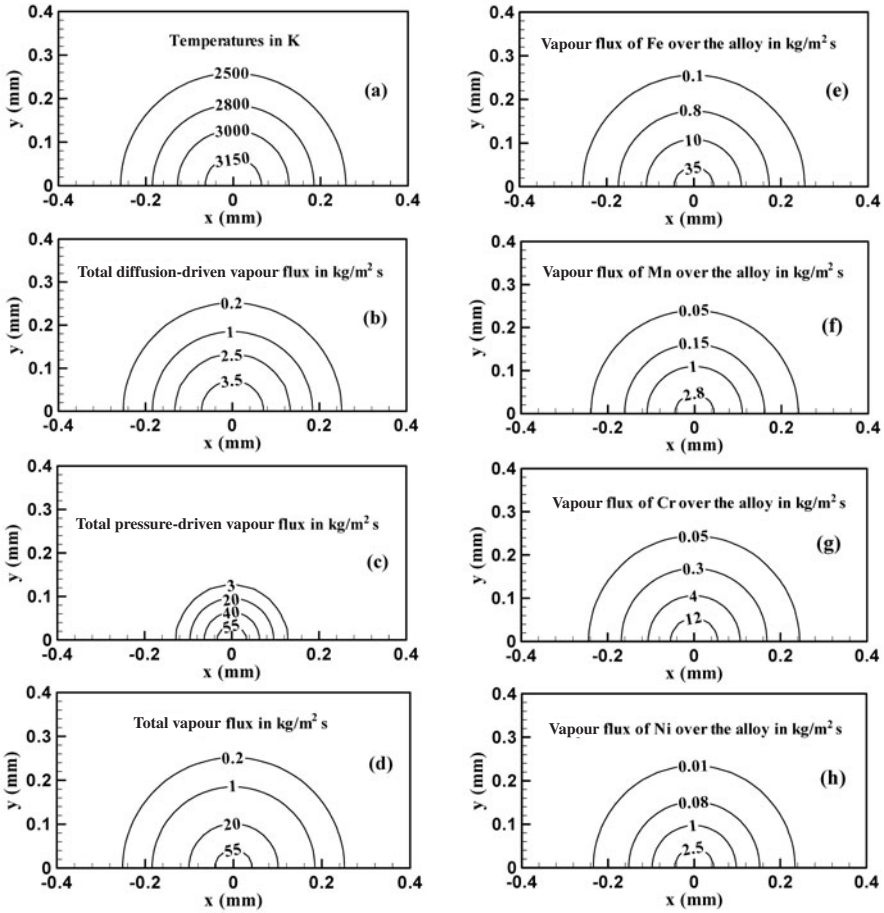

Figure 8. Distributions of temperature and vapour fluxes of various elements at the weld pool surface after 3.0 ms. Laser power: 1967 W, pulse duration: 3.0 ms, and beam radius: 0.428 mm.

The computed vaporization rates may be lower than the actual values because of several reasons. First, the computed temperatures on the weld pool surface may be lower than the actual values. Second, the computed weld pool surface area considered in the calculations is lower than the true surface area. Third, the vaporization model used in the calculations may underpredict the vaporization rate for the conditions of the current experiments. First, let us consider the possibility that the computed surface temperatures are lower than the actual temperatures prevailing at the surface. It has been established in several previous studies that during laser welding, most of the vapours originate from the centre of the weld pool surface [11, 12]. So, for the purpose of this inquiry, the magnitude of the computed peak temperature should be a good parameter to examine. The computed values of peak temperatures for all experiments are presented in table 4. The highest computed peak temperature listed in this table is 3628 K, which is about 600 K higher than the boiling point of the alloy. Although temperatures higher than the boiling point have been reported in [11, 12, 38–40], the reported temperatures are not significantly different from the boiling points for power densities close to about 10^6 W cm^{-2}. Therefore, the value of 3628 K, if deemed inaccurate for the sake of argument, can only be higher than the actual value. Furthermore, table 4 shows that even a temperature as high as 3628 K would not result in a vaporization rate necessary to account for all the mass loss due to vaporization. Therefore, the difference between the calculated and the experimental mass losses cannot be attributed to the lower computed temperatures. Second, let us examine the role of the weld pool surface area. When the recoil force of the vapours is significant, considerable depression of the weld pool free surface can result and the true surface area of the weld pool can be significantly higher than the nominal, flat, undeformed surface area. However, the deformation of the surface area can only account for a roughly 5–20% increase of the surface area for typical surface deformation. The data in table 4 show that the computed mass loss is significantly lower than the experimentally determined mass loss for most situations and that typical errors in the surface area cannot explain the difference. Third, the accuracy of the evaporation rate calculation must also be examined. The evaporation model has been adapted from the works of Anisimov [19] and Knight [20]. The same model has been extensively applied to calculate the laser-induced vaporization rates of alloying elements [11, 12, 40]. In each case, the computed vaporization rate was comparable with the corresponding experimental data. So, the difference between the computed vaporization loss and the experimental mass loss cannot be attributed to the inaccuracies resulting from the evaporation model. It is also worth noting that the experimentally measured mass loss indicated in table 4, if totally attributed to vaporization, demands unrealistically high values of vaporization rates. For

example, let us consider the experiment with a 0.159 mm radius laser beam having 530 W power applied for 4 ms. The total mass loss was found to be 15.6 μg. If the entire mass loss is attributed to vaporization, the vaporization rate can be readily estimated. If we assume that roughly 1 ms was needed for the initial heating, the average vaporization rate is calculated as 5.2 mg s^{-1}. For welding of stainless steel with a comparable power density beam, an overall vaporization rate of about 1 mg s^{-1} has been reported [13]. Thus, the experimental value of mass loss is far too high to be explained by vaporization alone.

A possible reason for the observed discrepancy between the experimental weight loss and the calculated vaporization loss is that only a portion of the mass loss occurs due to evaporation and the remainder of the loss must be attributed to some other mechanism. Therefore, the possibility of ejection of the tiny metal droplets from the weld pool owing to the recoil force exerted by the metal vapours was examined.

Expulsion of metal drops takes place when the vapour recoil force exceeds the surface tension force of the liquid metal at the periphery of the weld pool [40]. The vapour recoil force, F_r, and the surface tension force at the periphery, F_s, can be expressed by

$$F_r = 2\pi \int_0^{r_B} r \Delta P(r)\, dr \tag{9}$$

and

$$F_s = 2\pi r_0 \sigma \tag{10}$$

where r_B is the radial distance at which the surface temperature reaches the boiling point, $\Delta P(r)$ is the difference between the local equilibrium vapour pressure and the atmosphere pressure and is a function of radial distance from the beam axis, r_0 is the radial distance at which the temperature is equal to the melting point, and σ is the surface tension coefficient at the melting point. Figure 12 shows the computed values of these two forces during welding. As the temperature increases with time, the equilibrium vapour pressure and the resulting recoil force increase significantly. At about 1.4 ms after the start of the pulse, the two forces are roughly equal. Further heating results in a recoil force higher than the surface tension force. When the recoil force exceeds the surface tension force, ejection of metal droplets is anticipated. To verify the model prediction of metal droplet ejection, a few experiments were conducted where both end open quartz tubes were placed co-axial to the laser beam and right above the 304 stainless steel sample during the laser spot welding. The interior surface of the tube was examined after the experiments. Figure 13 shows the presence of metal vapour and tiny metal droplets on the interior wall of a quartz tube. Several small droplets can be seen in this macrograph. Clearly, mass loss is contributed by both vaporization of alloying elements and the ejection of metal droplets.

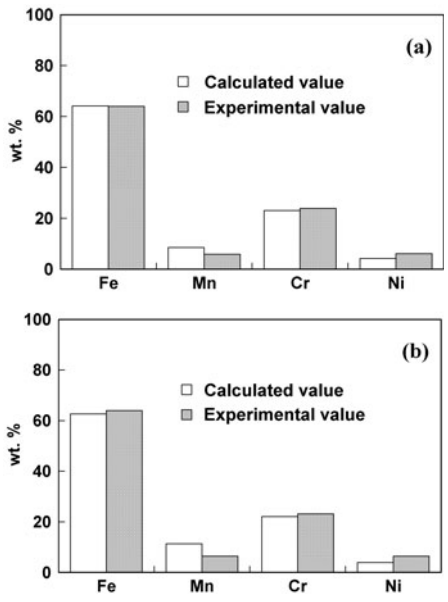

Figure 9. Weight per cent of different elements in vapour composition. (*a*) Laser power: 1063 W, pulse duration: 3.0 ms, and beam radius: 0.28 mm. (*b*) Laser power: 530 W, pulse duration: 4.0 ms, and beam radius: 0.171 mm.

5. Summary and conclusions

Loss of alloying elements from the weld pool during laser spot welding of stainless steel was investigated experimentally and theoretically. The experiments involved measurements of weight loss resulting from welding and analysis of the chemical composition of the vapour by condensing a portion of it on the inner surface of a both end open quartz tube. The theoretical work involved numerical modelling of transient temperature and velocity fields in the weldment and calculation of the vaporization rate of the alloying elements using the computed temperature profiles. The fusion zone geometry could be predicted from the transient heat transfer and fluid flow model for various welding conditions. In the range of variables investigated, the laser power and the pulse duration were

Table 3. The experimentally determined and calculated vapour composition for different welding conditions.

		Fe (%)		Mn (%)		Cr (%)		Ni (%)	
Spot radius (mm)		Exp	Cal	Exp	Cal	Exp	Cal	Exp	Cal
530 W, 4.0 ms	0.289	48.5	41.7	23.9	40.4	22.3	16.2	5.4	1.7
pulse	0.247	64.4	49.0	8.8	30.4	20.9	18.4	5.9	2.3
	0.227	57.6	52.6	7.4	25.5	20.4	19.3	14.7	2.6
	0.171	64.0	62.7	6.4	11.4	23.2	22.0	6.4	3.9
1063.3 W, 3.0 ms	0.326	67.1	58.6	8.1	17.5	18.8	20.7	6.0	3.3
pulse	0.28	64.0	64.2	5.9	8.5	23.9	23.1	6.2	4.2

'Exp' and 'Cal' indicate experimentally measured and calculated results, respectively.

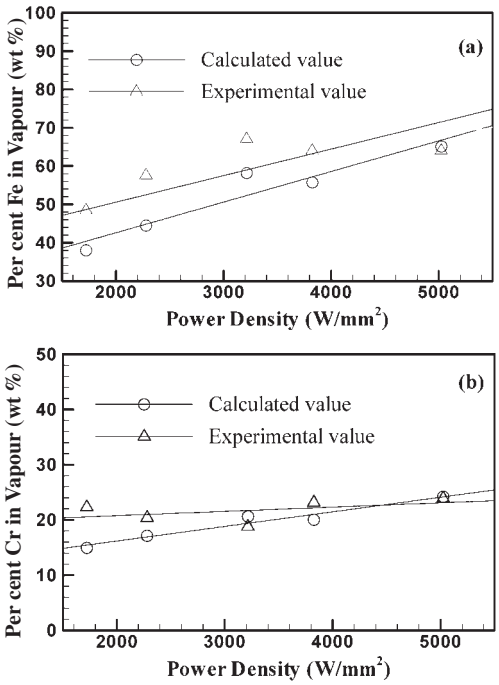

Figure 10. Experimental and computed concentrations of (*a*) Fe and (*b*) Cr in the vapour.

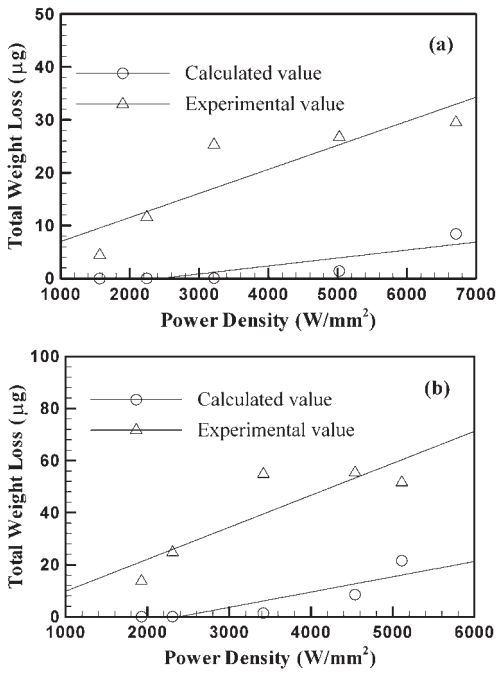

Figure 11. The calculated vaporization loss is compared with measured mass loss for different power densities. (*a*) Laser power: 1067 W and pulse duration: 3.0 ms. (*b*) Laser power: 1967 W and pulse duration: 3.0 ms.

Table 4. The calculated mass loss due to evaporation is compared with the experimentally determined mass loss for different welding conditions.

Spot radius (mm)		Calculated peak temperature (K)	Weight loss (μg) Calculated	Experimental
1967 W, 3.0 ms pulse	0.350	3628	21.52	51.6
	0.379	3448	8.50	55.3
	0.428	3205	1.42	54.8
	0.521	2814	0.08	24.7
	0.570	2674	0.04	13.7
1067 W, 3.0 ms pulse	0.225	3561	8.43	29.5
	0.260	3270	1.42	26.7
	0.325	2879	0.07	25.3
	0.389	2606	0.02	11.6
	0.466	2365	4.7×10^{-3}	4.4
530 W, 4.0 ms pulse	0.159	3176	0.46	15.6
	0.210	2761	0.03	3.6
	0.272	2451	6.7×10^{-3}	1.6
	0.313	2308	3.0×10^{-3}	0.6
	0.433	2032	0.5×10^{-3}	0.33

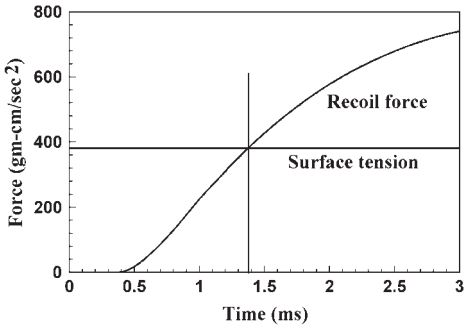

Figure 12. Recoil and surface tension forces as a function of time. Laser power: 1067 W, pulse duration: 3.0 ms, and beam radius: 0.225 mm.

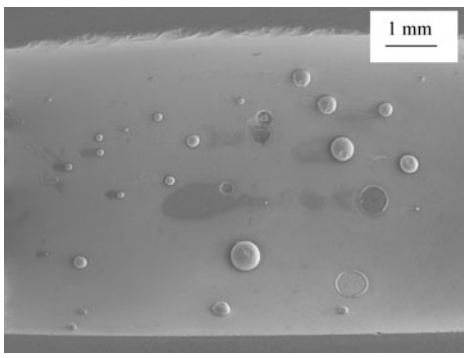

Figure 13. Particles of 304 stainless steel, ejected from the weld pool, were captured on the inner surface of a both end open quartz tube placed co-axial with the laser beam during spot welding. Laser power: 1967 W, pulse duration: 3.0 ms, and beam radius: 0.251 mm.

the most important variables in determining the temperature profile. During heating, temperatures and velocities increased with time, and convection played an increasingly important role in the heat transfer within the weld pool. The peak temperatures and velocities increased significantly with the laser power density. At very high power densities, the computed temperatures at the weld pool surface were found to be higher than the boiling point of 304 stainless steel. As a result, vaporization of alloying elements resulted from both total pressure and concentration gradients. The calculations showed that the vaporization was concentrated in a small region under the laser beam, where the temperature was very high. The computed vapour loss was found to be lower than the

measured mass loss because of the ejection of the tiny metal droplets owing to the recoil force exerted by the metal vapours. The ejection of metal droplets was predicted by computations and verified by experiments.

Acknowledgments

The work was supported by a grant from the US Department of Energy, Office of Basic Energy Sciences, Division of Materials Sciences, under grant number DE-FGO2-01ER45900. Portions of this work, performed at Sandia National Laboratories, were supported by US Department of Energy's National Nuclear Security Administration under contract DE-AC04-94AL85000. The authors would like to thank Jerome Norris and Paul Hlava for their help with the experimental measurements. The authors thank Mr Wei Zhang, Mr Amit Kumar, Mr Yajun Fan, Dr C L Kim, and Dr Amitava De for their valuable critical comments on various drafts of this manuscript.

Appendix. Equilibrium vapour pressure data used for the calculations

The equilibrium vapour pressures of the various vaporizing species over pure liquid were calculated using the following equations [41–44]. In these equations, the vapour pressure is expressed in atm and the temperature is in K.

$$\log(P^0_{\mathrm{Fe}} \times 760) = 11.5549 - 1.9538 \times 10^4 \frac{1}{T} - 0.625\,49 \log T - 2.7182 \times 10^{-9} T + 1.9086 \times 10^{-13} T^2$$

$$\log(P^0_{\mathrm{Mn}} \times 1.013 \times 10^5) = -5.58 \times 10^{-4} T - 1.503 \times 10^{-4} \frac{1}{T} + 12.609$$

$$\log(P^0_{\mathrm{Cr}} \times 1.013 \times 10^5) = -13.505 \times 10^3 \frac{1}{T} + 33.658 \log T - 9.29 \times 10^{-3} T + 8.381 \times 10^{-7} T^2 - 87.077$$

and

$$\log P^0_{\mathrm{Ni}} = 6.666 - 20\,765 \frac{1}{T}$$

Assuming that the solution is ideal at high temperatures, the equilibrium vapour pressures of the various species over the alloy can be expressed as

$$P_i = X_i P^0_i$$

where X_i is the mole fraction of element i in the alloy and P^0_i is the equilibrium vapour pressure of element i over the pure liquid.

References

[1] David S A and DebRoy T 1992 *Science* **257** 497
[2] Dunn G J, Allemand C D and Eagar T W 1986 *Metall. Trans.* A **17** 1863
[3] Dunn G J and Eagar T W 1986 *Metall. Trans.* A **17** 1871
[4] Blake A and Mazumder J 1985 *J. Eng. Indust.* **107** 275
[5] Sahoo P, Collur M M and DebRoy T 1988 *Metall. Trans.* B **19** 967
[6] Mundra K, Blackburn J M and DebRoy T 1997 *Sci. Technol. Weld. Joining* **2** 174
[7] Palmer T A and DebRoy T 2000 *Metall. Trans.* B **31** 1371
[8] Collur M M, Paul A and DebRoy T 1987 *Metall. Trans.* B **18** 733
[9] Moon D W and Metzbower E A 1983 *Weld. J.* **62** 53s
[10] Cieslak M J and Fuerschbach P W 1988 *Metall. Trans.* B **19** 319
[11] Zhao H and DebRoy T 2001 *Metall. Trans.* B **32** 163
[12] Mundra K and DebRoy T 1993 *Metall. Trans.* B **24** 145
[13] Khan P A A, DebRoy T and David S A 1988 *Weld. J.* **67** 1s
[14] Khan P A A and DebRoy T 1984 *Metall. Trans.* B **15** 641
[15] Mundra K and DebRoy T 1993 *Weld. J.* **72** 1s
[16] Block-bolten A and Eager T W 1984 *Metall. Trans.* B **15** 461
[17] Aden M, Beyer E, Herziger G and Kunze H 1992 *J. Phys. D: Appl. Phys.* **25** 57
[18] Dilthey U, Goumeniouk A, Lopota V, Turichin G and Valdaitseva E 2001 *J. Phys. D: Appl. Phys.* **34** 81
[19] Anisimov S I and Rakhmatulina A Kh 1973 *Sov. Phys.—JETP* **37** 441
[20] Knight C J 1979 *AIAA J.* **17** 519
[21] Chun M K and Rose K 1970 *J. Appl. Phys.* **11** 614
[22] Graham M P, Kerr H W and Weckman D C 1996 *Proc. SPIE—The International Society for Optical Engineering* (San Jose, CA) vol 2703, p 170
[23] von Allmen M 1976 *J. Appl. Phys.* **47** 5460
[24] Basu S and DebRoy T 1992 *J. Appl. Phys.* **72** 3317
[25] He X, Fuerschbach P W and DebRoy T 2003 *J. Phy. D: Appl. Phys.* **36** 1388
[26] Zhang W, Roy G, Elmer J and DebRoy T 2003 *J. Appl. Phys.* **93** 3022
[27] Yang Z, Sista S, Elmer J W and DebRoy T 2000 *Acta Mater.* **48** 4813
[28] Hong T, DebRoy T, Babu S S and David S A 2000 *Metall. Trans.* B **31** 161
[29] Zhang W, Elmer J W and DebRoy T 2002 *Mater. Sci. Eng.* A **333** 320
[30] Fuerschbach P W and Norris J T 2002 Beam characterization for Nd : YAG spot welding lasers *International Conf. on Application of Lasers and Electro-Optics 2002 (Scottsdale, AZ)*
[31] Peckner D and Bernstein I M 1977 *Handbook of Stainless Steels* (New York: McGraw-Hill)
[32] Davis J R 1998 *Metals Handbook* (Materials Park, OH: ASM International)
[33] Davis J R 1994 *ASM Specialty Handbook. Stainless Steel* (Materials Park, OH: ASM International)
[34] ASM International Handbook Committee 1990 *Metals Handbook. Volume 1. Properties and Selection: Ion, Steels, and High-Performance Alloys* (Materials Park, OH: ASM International)
[35] Schlunder E U and Gniclinski V 1967 *Chem. Eng. Technol.* **39** 578
[36] Iida T and Guthrie R I L 1988 *The Physical Properties of Liquid Metals* (Oxford: Clarendon) p 8
[37] Richardson F D 1974 *Physical Chemistry of Melts in Metallurgy* (London: Academic)
[38] Chan C L and Mazumdar J 1987 *J. Appl. Phys.* **62** 4579
[39] von Allmen M 1987 *Laser Beam Interaction with Materials* (Berlin: Springer) p 161
[40] DebRoy T, Basu S and Mundra K 1991 *J. Appl. Phys.* **70** 1313
[41] Hultgren R, Desai P D, Hawkins D T, Gleiser M, Kelley K K and Wagman D D 1973 *Selected Values of the Thermodynamic Properties of the Elements* (Materials Park, OH: ASM International)
[42] Honig R E and Kramer D A 1970 *Physicochemical Measurements in Metal Research* (New York: Interscience) p 505
[43] Yaws C L 1994 *Handbook of Vapor Pressure* (Houston: Gulf)
[44] Alcock C B, Itkin V P and Horrigan M K 1984 *Can. Metall. Q.* **23** 309